RESEARCH ARTICLE SUMMARY

PALEOBIOLOGY

Quantifying the global biodiversity of Proterozoic eukaryotes

Qing Tang*, Wentao Zheng, Shuhan Zhang, Junxuan Fan, Leigh Anne Riedman, Xudong Hou, A. D. Muscente, Natalia Bykova, Peter M. Sadler, Xiangdong Wang, Feifei Zhang, Xunlai Yuan, Chuanming Zhou, Bin Wan, Ke Pang*, Qing Ouyang, N. Ryan McKenzie, Guochun Zhao, Shuzhong Shen*, Shuhai Xiao*

INTRODUCTION: The Proterozoic Eon [2500 to 539 million years ago (Ma)] in Earth history is marked by numerous transformative evolutionary, environmental, and tectonic events. However, a comprehensive quantification of Proterozoic eukaryote fossil diversity is lacking, hampering analysis of the global patterns and mechanisms of Earth-life coevolution in this important eon. Here we report a high-resolution analysis of the diversity and evolutionary dynamics of Proterozoic and early Cambrian (539 to 509 Ma) eukaryotes based on a global compilation of fossil data. This result provides opportunities to test various hypotheses about the coevolution of the Proterozoic biosphere and geosphere.

RATIONALE: The graphic correlation program Constrained Optimization (CONOP) was used to optimize correlations across fossiliferous sections and to develop the best-fit composite sequence of the first and last appearances of fossil species. The CONOP computation was supplemented by geologically correlatable events and time-calibrated by radiometric ages. The diversity of Proterozoic and early Cambrian eukaryote fossils was then calculated from the composite sequence, with various sensitivity tests to assess the impact of uncertain age estimates, ambiguous taxonomic assignments, putative eukaryotic affinities, and fossil sampling biases on the estimate of global species richness.

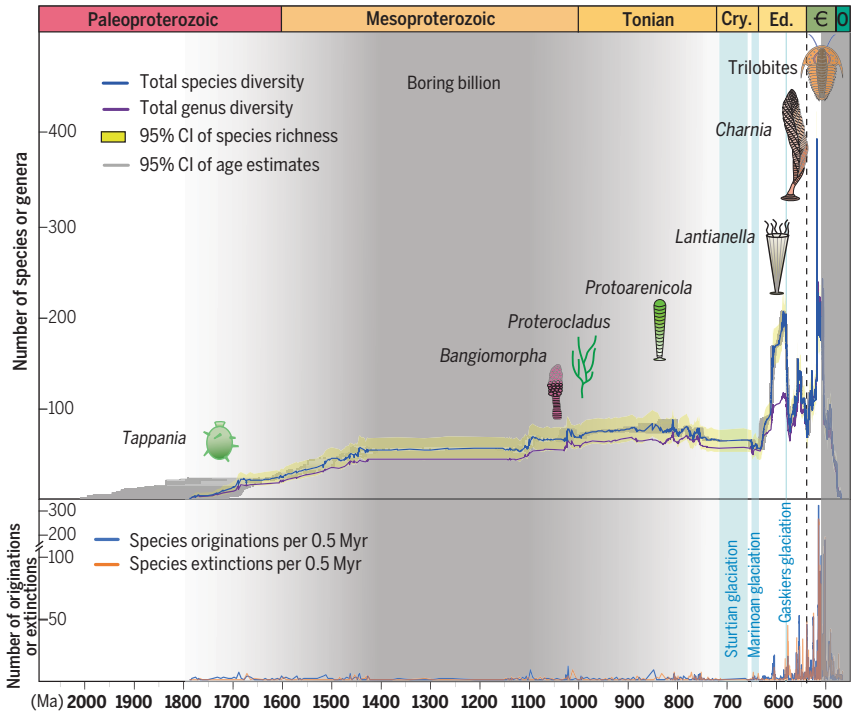

Evolutionary patterns and dynamics of Proterozoic and early Cambrian eukaryotes. (Top) Taxonomic richness of eukaryotic fossils (sketches depict representative fossils). (Bottom) Species origination and extinction rates. Note scale change at 100 on the vertical axis. Vertical light-gray, blue, and dark-gray bars denote the "Boring Billion," glacial intervals, and the buffer zone due to edge effects, respectively. Cry., Cryogenian; Ed., Ediacaran; Є, Cambrian; O, Ordovician; CI, confidence interval; Myr, million years.

RESULTS: The results confirm the Cryogenian Period (~720 to 635 Ma) as a major divide in Proterozoic eukaryote evolution. The species richness of eukaryote fossils remained consistently low and relatively static with small-scale fluctuations before the Cryogenian but increased rapidly and experienced more dynamic changes in the Ediacaran (~635 to 539 Ma) and early Cambrian periods. Similarly, species origination, extinction, and turnover rates were low before the Ediacaran Period but were much higher and showed greater variation afterward. The accelerated evolutionary dynamics are exemplified by the rapid rise and fall of various groups of Ediacaran eukaryotes, including the rapid decline of a group of Ediacaran microfossils known as the Doushantuo-Pertatataka acritarchs (DPAs) after the Gaskiers glaciation (~581 to 580 Ma), the subsequent diversification of the Ediacara biota that is represented by Ediacara-type macrofossils and includes some of the earliest known macroscopic animals, and double extinctions at ~551 Ma and 542 to 539 Ma that led to the demise of the Ediacara biota.

CONCLUSION: The quantitative results provide critical insights into the coevolution of Earth and life in the Proterozoic Eon. The contrasting evolutionary patterns of eukaryotes before and after Cryogenian glaciations indicate that global glaciations played an important role in the macroevolution of Proterozoic eukaryotes. The static diversity pattern before the Cryogenian Period echoes the "Boring Billion" (~1800 to 800 Ma), which is characterized by stability in the global carbon cycles. Considering that major eukaryotic groups may have diverged in the "Boring Billion," there must have been a long delay before Proterozoic eukaryotes rose to ecological and taxonomic dominance. In the Ediacaran Period, the rapid disappearance of DPAs that began during the Gaskiers glaciation represents the earliest mass extinction of eukaryotes in the Proterozoic Eon, probably due to global cooling. The rise of macroscopic animals and their traces coincided with the nadir of the Shuram excursion (574 to 567 Ma) that represents the largest perturbation to the carbon cycle in Earth history, indicating a possible causal relationship between oceanic oxygenation and the rise of macroscopic animals. The double extinctions in the late Ediacaran Period represent the first documented mass extinctions of animals. These evolutionary events highlight the complex interplay in the Proterozoic Earth-life system. ■

The list of author affiliations is available in the full article online.
*Corresponding author. Email: qingt@nju.edu.cn (Q.T.); kepang@nigpas.ac.cn (K.P.); szshen@nju.edu.cn (S.S.); xiao@vt.edu (S.X.)
Cite this article as Q. Tang *et al.*, *Science* **386**, eadm9137 (2024). DOI: 10.1126/science.adm9137

READ THE FULL ARTICLE AT
https://doi.org/10.1126/science.adm9137

RESEARCH ARTICLE

PALEOBIOLOGY

Quantifying the global biodiversity of Proterozoic eukaryotes

Qing Tang[1,2,3]*, Wentao Zheng[4], Shuhan Zhang[1], Junxuan Fan[1], Leigh Anne Riedman[4], Xudong Hou[1], A. D. Muscente[5], Natalia Bykova[6,7], Peter M. Sadler[8], Xiangdong Wang[1], Feifei Zhang[1], Xunlai Yuan[9], Chuanming Zhou[9], Bin Wan[9], Ke Pang[9]*, Qing Ouyang[9], N. Ryan McKenzie[3], Guochun Zhao[3,10], Shuzhong Shen[1]*, Shuhai Xiao[2]*

The global diversity of Proterozoic eukaryote fossils is poorly quantified despite its fundamental importance to the understanding of macroevolutionary patterns and dynamics on the early Earth. Here we report a new construction of fossil eukaryote diversity from the Paleoproterozoic to early Cambrian based on a comprehensive data compilation and quantitative analyses. The resulting taxonomic richness curve verifies Cryogenian glaciations as a major divide that separates the "Boring Billion" and Ediacaran periods, with the former characterized by a prolonged stasis, and the latter by greater diversity, more-rapid turnover, and multiple radiations and extinctions. These contrasting evolutionary patterns and dynamics provide a framework to test competing hypotheses on biosphere and geosphere coevolution in the Proterozoic Eon.

Quantifying the global diversity of fossils can reveal the evolutionary trajectory of life (*1*) and inform causal relationships between biotic turnover and environmental changes (*2*, *3*), as exemplified by the well-known mass extinctions and associated environmental perturbations in the Phanerozoic Eon (*2*, *4*–*7*). The Proterozoic is also marked by transformative tectonic and environmental changes, including the assembly and disassembly of supercontinents (*8*), major shifts in atmospheric and oceanic chemistry (*9*), and the most extensive icehouse climate (*10*). However, quantitative understanding of global fossil diversity of Proterozoic life, particularly eukaryotes, remains incomplete, limited in scope, and plagued with inconsistent taxonomic treatments and poorly defined age constraints. These deficiencies render the Proterozoic evolutionary history a largely qualitative narrative, substantially limiting our ability to decipher the evolutionary patterns and dynamics of early eukaryotes and the coevolution between the Proterozoic biosphere and geosphere.

In the past few decades, there have been several attempts to explore the Proterozoic diversity patterns of eukaryotic fossils using metrics of binned taxonomic richness (*11*, *12*), morphological disparity (*13*, *14*), and within-assemblage diversity (*12*, *15*, *16*). However, because they did not leverage stratigraphic occurrence data, these assessments were compromised by coarse and uneven age bins. The lack of statistical tests on the effects of sampling biases further complicates the interpretation of the quantitative results (*17*). Moreover, notable expansions of Proterozoic paleontological and geochronological data in the past decade [e.g., (*18*–*20*)] (figs. S1 to S3) necessitate a reassessment of Proterozoic biodiversity on the basis of a more comprehensive database and advanced analytical techniques such as the Constrained Optimization (CONOP) algorithm, which has been shown to substantially improve the quantification of Phanerozoic (*2*, *21*) and Neoproterozoic (*17*) fossil diversity. By incorporating biostratigraphic, chronostratigraphic, chemostratigraphic, and lithostratigraphic data from all target sections, CONOP has the advantage of circumventing the need for age constraints on all sections and thus including undated or poorly dated fossiliferous sections in the correlation (*22*). As a result, the temporal resolution of the resulting composite section, and hence that of biodiversity patterns and dynamics, can be substantially improved by CONOP computation (*2*).

Here we report a new construction of fossil eukaryotic species richness over the Proterozoic and early Cambrian using a parallel computing implementation of the CONOP program (CONOP.Para). Based on a global compilation of fossil eukaryotes and thorough analyses to address sampling biases and various uncertainties in taxonomic assignments, phylogenetic interpretations, and radiometric dates, our study generated a high-resolution diversity curve of Proterozoic eukaryotic fossils, providing a valuable window onto evolutionary patterns and dynamics of early eukaryotes. These results offer opportunities to test various hypotheses about the coevolution of the Proterozoic biosphere and geosphere.

Results

The best-fit composite sequence

The dataset [data S1 (*23*)] covered the Proterozoic and early Cambrian, comprising 263 stratigraphic sections, 15 pseudosections, and 13,658 events (i.e., local or section-level occurrences of stratigraphic features regarded as time markers). Of these events, there were 12,820 local first appearance datum (FAD) and last appearance datum (LAD) records of 2731 species assigned to four eukaryotic fossil groups [data S1 (*23*)], 185 radiometric ages [220 events; sometimes, one radiometric age is assigned to multiple sections that can be correlated with a high level of confidence, e.g., the 635 million year (Myr) age from the top of the Doushantuo cap dolostone], 35 biozonal species with 52 FAD and LAD occurrences (210 events), 10 sedimentological mark beds (135 events), 22 geochemical excursions including the rise, peak, and fall of each (202 events), and 36 pseudoevents (71 events). Of the 2731 species, 776 were classified as unicellular eukaryotes, 206 as multicellular or coenocytic eukaryotes, 1617 as animal body fossils, and 132 as animal trace fossils.

The best-fit composite sequence was based on the CONOP solution with the lowest required adjustment of all local ranges (Fig. 1A). It consists of 1258 fossiliferous temporal levels [i.e., counting points in (*2*), or temporal levels with one or more FADs or LADs] in the study interval between 2087 and 509 million years ago (Ma) (excluding the buffer zone; Fig. 1A). Hence, the nominal total average temporal resolution is (2087 – 509 Ma)/1258 = 1.25 Myr, with the average temporal resolution in the Proterozoic, pre-Ediacaran, Ediacaran, and early Cambrian at ~2.17, ~6.57, ~0.19, and ~0.06 Myr, respectively. These are all nominal average temporal resolutions given the existences of large variations in different Proterozoic periods.

General trajectory of diversity pattern

The species richness curve confirms the Cryogenian Period as a major divide in the diversity pattern of early eukaryotic fossils (*24*). In the pre-Cryogenian Proterozoic, roughly corresponding to the "Boring Billion" (*25*) or "Balanced Billion" (*26*) from ~1800 to ~800 Ma, taxonomic richness was consistently low and relatively static (Fig. 1, A and B). Small-scale

[1]State Key Laboratory for Mineral Deposits Research, School of Earth Sciences and Engineering, and Frontiers Science Center for Critical Earth Material Cycling, Nanjing University, Nanjing, China. [2]Department of Geosciences and Global Change Center, Virginia Tech, Blacksburg, VA, USA. [3]Department of Earth Sciences, University of Hong Kong, Hong Kong, China. [4]Department of Earth Science, University of California, Santa Barbara, Santa Barbara, CA, USA. [5]Princeton Consultants, Princeton, NJ, USA. [6]Department of Geological Sciences, University of Missouri, Columbia, MO, USA. [7]Trofimuk Institute of Petroleum Geology and Geophysics of Siberian Branch of Russian Academy of Sciences, Novosibirsk, Russia. [8]Department of Earth Sciences, University of California, Riverside, Riverside, CA, USA. [9]State Key Laboratory of Palaeobiology and Stratigraphy, Nanjing Institute of Geology and Palaeontology, Chinese Academy of Sciences, Nanjing, China. [10]State Key Laboratory of Continental Dynamics, Department of Geology, Northwest University, Xi'an, China.
***Corresponding author. Email: qingt@nju.edu.cn (Q.T.); kepang@nigpas.ac.cn (K.P.); szshen@nju.edu.cn (S.S.); xiao@vt.edu (S.X.)**

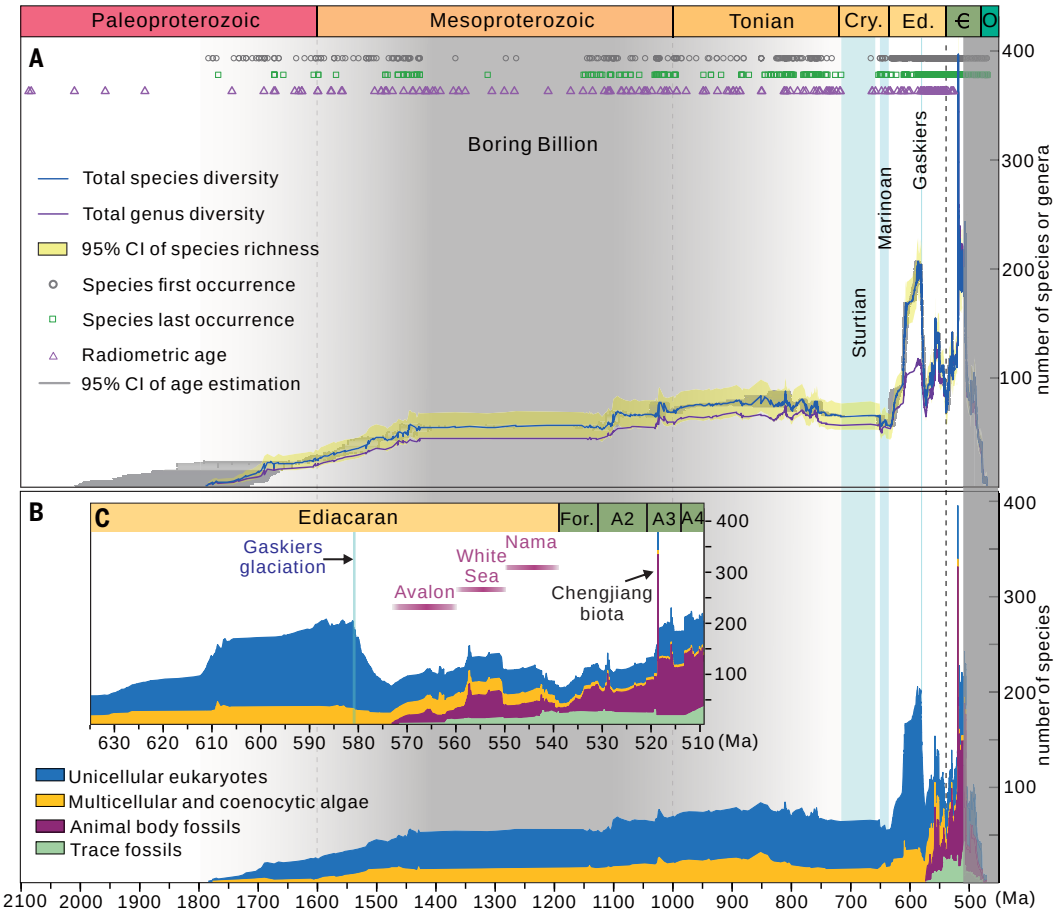

Fig. 1. Biodiversity trajectory of eukaryotic fossils from the Paleoproterozoic to early Cambrian. (**A**) Genus and species richness curves, first and last occurrences of species, and Proterozoic radiometric ages applied in the Bayesian age-depth model of this study. See figs. S9 and S10 and data S2 (*23*) for data plotted in this figure. The median ages from the age model were applied to construct the total genus and species diversity curves. Gray horizontal bars denote the associated 95% confidence intervals of modeled median ages at each temporal level. The yellow shading represents the 95% confidence interval from bootstrapping all species after CONOP analysis of the full dataset. (**B**) Stacked species richness of major eukaryotic groups in the study interval. In (A) and (B), light-gray shading with fading boundaries denotes the "Boring Billion" interval, light-blue vertical bars represent the three Neoproterozoic glacial intervals, and the dark-gray vertical bar at the right of the panel marks the buffer zone reflecting the edge effect (see materials and methods). (**C**) Stacked species richness of major eukaryotic groups in Ediacaran–early Cambrian (635 to 509 Ma). Purple horizontal bars denote the three Ediacara-type macrofossil assemblages: Avalon, White Sea, and Nama assemblages. The Chengjiang spike is truncated, but its value can be seen in (A). CI, confidence interval; Cry., Cryogenian; Ed., Ediacaran; Є, Cambrian; O, Ordovician; For., Fortunian; A2, A3, and A4, Cambrian Ages 2, 3, and 4, respectively.

changes did occur in the "Boring Billion," including a slow but steady increase in species richness from the Paleoproterozoic to the Tonian. There are also several stepwise increases in the late Paleoproterozoic, early and late Mesoproterozoic, and late Tonian. Species richness then slightly dropped before the Tonian-Cryogenian boundary and again in the terminal Cryogenian Period.

Eukaryotic fossil diversity climbed rapidly and experienced more dynamic fluctuations in the Ediacaran Period. A species-richness peak occurred in the early Ediacaran, followed by a substantial decline beginning at the Gaskiers glaciation (~581 to 580 Ma) (*27*), with a loss of ~64% species in the following ~8 Myr. This was followed by another sharp increase peaking at ~557 Ma and two decreases starting at ~551 and ~544 Ma (Fig. 1C), leading to a diversity nadir at the Precambrian-Cambrian boundary (~539 Ma). The species richness recovered rapidly in the early Cambrian, with an unprecedented richness in Cambrian Age 3. Genus-level richness shows patterns and trends similar to those of species-level richness, with an expectedly lower number of genera than species (Fig. 1A).

Partition of species richness among major eukaryotic groups

The four major eukaryotic fossil groups in our dataset (i.e., unicellular eukaryotes, multicellular and coenocytic algae, animal body fossils, and trace fossils) exhibit different richness patterns over the study interval (Fig. 1, B and C). Unicellular eukaryotes and multicellular or coenocytic eukaryotes dominated the eukaryotic fossil diversity, and their richness patterns were similar to those of total eukaryotic species richness before the Gaskiers glaciation. The species diversity of unicellular eukaryotic fossils then experienced an unprecedented 70% decline in the next ~8 Myr, remained stable thereafter until another minor decline near the Precambrian-Cambrian boundary, and gradually rebounded in the early Cambrian (Fig. 1C). In contrast, the fossil richness pattern of multicellular or coenocytic eukaryotes only experienced a minor decline at 544 to 539 Ma. The initial rise of animal body fossils after the Gaskiers glaciation was followed by a notable increase in species richness peaking at ~557 Ma and two subsequent drops in the late Ediacaran. Animal body fossil diversity rebounded immediately after the Ediacaran-Cambrian boundary and had stepwise increases thereafter, with a richness peak in Cambrian Age 3. Finally, animal trace fossils first appeared around the same time as the first macroscopic animal body fossils. However, their species richness remained relatively low, with two small rises before the Ediacaran-Cambrian boundary, followed by minor fluctuations in the early Cambrian (Fig. 1C).

Diversity dynamics

Multiple metrics of evolutionary rates have been quantified to evaluate diversity dynamics of Proterozoic eukaryotes (Figs. 2 and 3 and

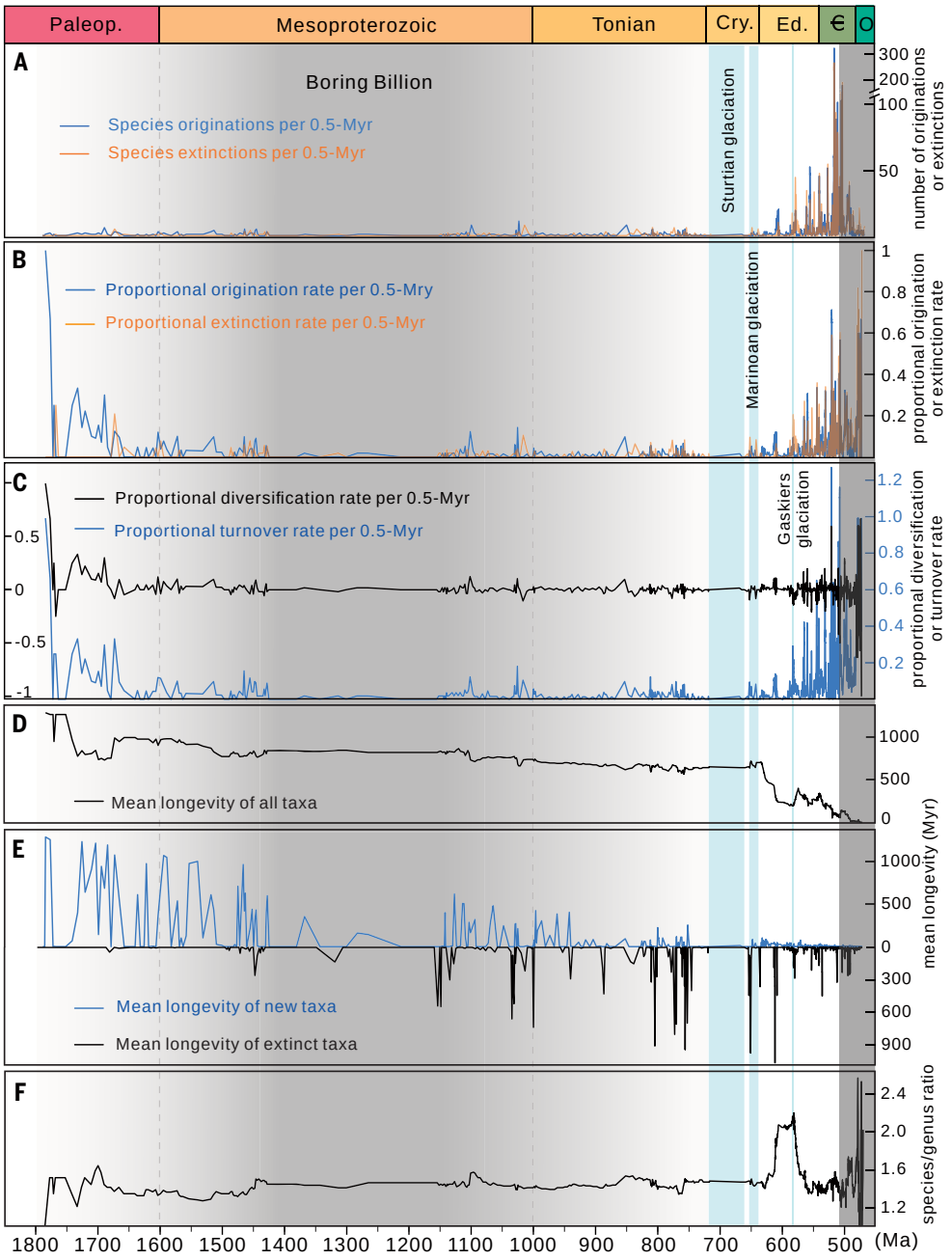

Fig. 2. Biodiversity dynamics of Proterozoic eukaryotes. (**A**) Origination and extinction rates measured at species per bin (= 0.5 Myr). Note scale change at 100 on vertical axis. (**B**) Proportional origination and extinction rates measured at per capita species per bin (= 0.5 Myr). (**C**) Proportional diversification and turnover rates per bin (= 0.5 Myr). (**D** and **E**) Mean longevity of all, new, and extinct species. (**F**) Species/genus ratio. Vertical bars and abbreviations are the same as in Fig. 1. Paleop., Paleoproterozoic. See data S2 (*23*) for data plotted in this figure.

figs. S4 to S5). Specifically, both the origination and extinction rates were low (<15 species per 0.5 Myr) before the Ediacaran and approached zero during much of the middle Mesoproterozoic owing to the dominance of long-ranging species and the relatively low number of FAD and LAD occurrences. In contrast, the two metrics showed much greater variations in the Ediacaran and early Cambrian. Additionally, the origination rate was generally higher than the extinction rate in the early Ediacaran but frequently lower than the extinction rate after the Gaskiers glaciation (Fig. 3B and fig. S5). During the early Cambrian, however, the origination rate was slightly greater than the extinction rate, particularly in Cambrian Age 1 and Age 3.

The per capita, or proportional, origination and extinction rates showed several phases. The late Paleoproterozoic is characterized by large-amplitude fluctuations, with the proportional origination rate generally higher than the proportional extinction rate. The Mesoproterozoic-to-Cryogenian is characterized by long-term stasis, with extremely low values of both rates, except for several minor fluctuations in the early and latest Mesoproterozoic and the late Tonian. And the Ediacaran-to-early Cambrian is characterized by rapid and large fluctuations of both rates, with relatively low values in early Ediacaran but much higher values after the Gaskiers glaciation (Figs. 2B and 3C). Similarly, both proportional diversification and turnover rates fluctuated prominently in the late Paleoproterozoic and subsequently became relatively static until the Ediacaran Period. These two rates became more dynamic in the Ediacaran, particularly after ~581 Ma (Figs. 2C and 3D), indicating accelerated evolutionary dynamics after the Gaskiers glaciation.

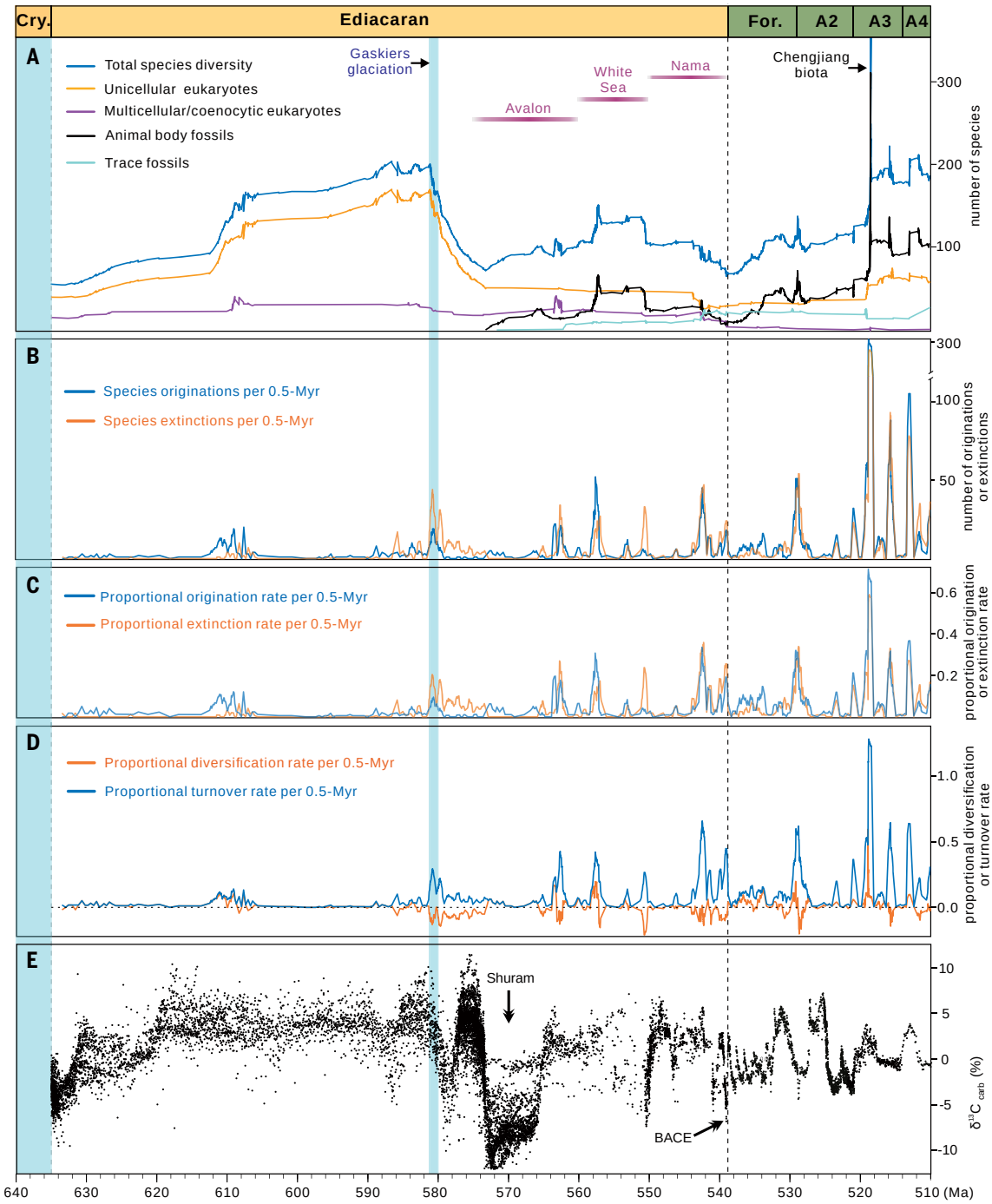

Fig. 3. Fossil eukaryote dynamics and $\delta^{13}C_{carb}$ of the Ediacaran and early Cambrian periods. (**A**) Species richness curves of major eukaryotic groups. This figure plots the same data as does Fig. 1C, but the curves are plotted individually rather than cumulatively as in Fig. 1C. The total species richness of the Chengjiang spike is truncated, but its value can be seen in Fig. 1A. (**B**) Origination and extinction rates measured in species per time bin (= 0.5 Myr). Note scale change at 100 on vertical axis. (**C**) Proportional origination and extinction rates in per capita species per time bin. (**D**) Proportional diversification and turnover rates in per capita species per time bin. (**E**) $\delta^{13}C_{carb}$ profile (*57*, *73*). BACE, basal Cambrian excursion. Vertical bars and abbreviations are the same as in Fig. 1.

The mean longevity of all taxa was inversely correlated with the species richness change, manifested as a first-order decreasing trend from the Paleoproterozoic to early Cambrian (Fig. 2D). This observation suggests that the average longevity of all taxa declined through time, a trend also observed in previous studies [e.g., (*12*)]. The mean longevity of new taxa also showed a generally decreasing trend in the study interval (Fig. 2E), suggesting that species that originated earlier tend to have longer stratigraphic ranges than those that

came later. In contrast, the mean longevity of extinct taxa had extremely low values before the early Mesoproterozoic (>~1450 Ma), gradually increased between ~1450 Ma and ~610 Ma, and subsequently decreased sharply after ~610 Ma (Fig. 2E), mainly because of the preferential extinction of species with long stratigraphic ranges. The longevity patterns are consistent with other evolutionary dynamics measured in origination, extinction, and turnover rates (Fig. 2, A to C), which all showed an overall increasing trend from the Paleoproterozoic to early Cambrian.

The species/genus ratio varied mostly between 1.2 and 1.5 before the Ediacaran and subsequently rose to between 1.5 and 2.2 in the early Ediacaran (Fig. 2F). The ratio declined considerably after ~581 Ma (Gaskiers glaciation) and fluctuated between 1.3 and 1.6 in the late Ediacaran and early Cambrian by 509 Ma. It is noteworthy that the species/genus ratio and the species richness pattern showed similar trends in the early Ediacaran, indicating that rapid within-genus origination and extinction contributed substantially to the eukaryotic radiation and subsequent extinction in the early Ediacaran. This observation suggests that species-level richness can provide additional information about biodiversity analyses that may be concealed in genus-level richness. Alternatively, the increase in species/genus ratio in the early Ediacaran could be a taxonomic artifact due to excessive species splitting. Finally, although the diversity reached an unprecedented level in Cambrian Age 3, the species/genus ratio was relatively low, indicating that the apex of the Cambrian explosion was mainly contributed by the rapid origination at the genus level, consistent with the traditional view that the Cambrian explosion was focused on high taxonomic levels (*28*).

Assessment of biases

A total of 12 independent CONOP runs were conducted to assess the robustness and stability of the best-fit composite sequence. These CONOP runs generated 12 nearly equally well-fit solutions and were time-calibrated using the Bchron Bayesian age-depth model and biozone species described in the materials and methods. The species richness patterns of these solutions are indistinguishable (fig. S6A), suggesting that the optimization was stable and the patterns of fossil diversity are robust.

The veracity of the species richness patterns was evaluated using multiple sample-standardization techniques, including bootstrapping (Fig. 1A), rarefaction analyses (fig. S6B), and section number standardization (fig. S6C). The bootstrapping analysis showed that the best-fit richness curve from CONOP analysis of the full dataset was within the 95% confidence interval (Fig. 1A). Additionally, the rarefied richness curves, even when the sample size was reduced to 200, captured the main features of the richness curve derived from CONOP analysis of the full dataset (fig. S6B). The standardized diversity curve (i.e., normalized against the number of sections) showed no notable changes from the species richness curve derived from CONOP analysis of the full dataset (fig. S6C), even though there are some fluctuations in the number of sections through time. This observation suggests that the general trajectory of the richness curve was not strongly influenced by the uneven number of sections. Therefore, these statistical tests suggested that the richness curve reconstructed from the best-fit composite sequence was robust and the effect of uneven sampling was minimal.

In addition, sensitivity tests were applied to include or exclude fossils with ambiguous taxonomic assignments (fig. S7A), controversial eukaryotic affinities (fig. S7B), or extremely short stratigraphic ranges mostly attributable to the Lagerstätte effect [fig. S7C; see the supplementary text in the supplementary materials (*29*)]. The result shows that the best-fit composite sequence of the dataset without open nomenclatures (e.g., xx sp., xx sp. A, xx sp. B, etc.) gave diversity patterns similar to those of the full dataset (fig. S7A), suggesting that the inclusion of open nomenclatures in our dataset did not systematically bias the total species diversity pattern. Similarly, a reanalysis of the full dataset excluding taxa tagged as "possible eukaryotes" (e.g., leiospheres and other simple forms) resulted in a similar fossil diversity pattern (fig. S7B). Besides, the temporal trends of the mean longevity for all, new, and extinct taxa and the origination and extinction rates did not change notably when the dataset was culled to exclude fossils with controversial eukaryotic affinities (i.e., tagged as "possible eukaryote") (fig. S4). The sensitivity test of the Lagerstätte effect showed that the prominent Chengjiang spike disappeared when short-lived taxa were excluded from the analysis (fig. S7C), suggesting that this spike was likely an artifact of exceptional preservation and intensive sampling of the Changjiang biota; however, all other features of the fossil curve remained the same, including the notable diversity increase in Cambrian Age 3 (fig. S7C), confirming the Cambrian radiation event. Thus, these analyses suggest minimal impact of fossils with ambiguous taxonomic assignments, controversial eukaryote affinities, and Lagerstätte effect on the general patterns of fossil diversity dynamics of Proterozoic eukaryotes.

Finally, an analysis of rock abundance was conducted to test preservational biases related to sedimentary processes (fig. S8). The rock abundance analysis showed little overall correlation between fossil species diversity and Macrostrat rock abundance when all data were pooled together [Pearson correlation coefficient (r) = ~0.06; fig. S8]. When viewed separately, there was a strong positive correlation in the early Cambrian and a strong negative correlation in the late Paleoproterozoic–early Mesoproterozoic (fig. S8). It is uncertain what these correlations mean, although it has been suggested that the positive correlation in the early Cambrian may have resulted from a common cause: major sea level rise and continental-scale transgression related to global tectonics (e.g., breakup of Gondwana) may have flooded large areas of continental shelves, creating accommodation for sediment accumulation and shelf environments where animal diversification occurred (*30*).

The generally low fossil diversity in the Mesoproterozoic–Cryogenian and the three plateaus in the fossil species richness curve (i.e., ~1400 to 1100 Ma, ~1000 to 890 Ma, and ~720 to 650 Ma; Fig. 1, A and B) warrant further discussion. In principle, such plateaus can be driven by incomplete fossil preservation, poor sampling, or low turnover rate. Indeed, the number of species first and last occurrences is low in the Mesoproterozoic–Cryogenian relative to that of Ediacaran–Cambrian, and particularly low in the intervals matching the three plateaus (Fig. 1A), consistent with a role of poor preservation or sampling. However, the origination, extinction, and turnover rates are also low in the Mesoproterozoic–Cryogenian relative to that of Ediacaran–Cambrian, and particularly low in the intervals matching the three plateaus (Fig. 2, A to C), suggesting that long-ranging taxa are at least partially responsible. In addition, thick shale and mudstone suitable for the fossil preservation are known in the Mesoproterozoic–Cryogenian (*31*–*34*) (fig. S8A), but fossiliferous strata from these intervals are generally dominated by long-ranging taxa (*35*–*39*). More importantly, our bootstrapping and rarefaction analyses showed that variations in incomplete fossil preservation or sampling alone do not account for the first-order trend of the species richness curve (Fig. 1A and fig. S6B). Thus, these observations indicate that the low levels of eukaryotic fossil occurrences likely reflect a genuinely low fossil diversity in the Mesoproterozoic–Cryogenian.

We note that Proterozoic eukaryotes were dominated by nonbiomineralizing organisms. Thus, many of them were not fossilizable and therefore left no fossils. While their potential biases cannot be assessed by post hoc analyses, there are no compelling reasons to believe that such biases are systematic or responsible for the observed patterns. The fossilization of Proterozoic nonbiomineralizing eukaryotes requires broadly similar taphonomic conditions. This broad uniformity stands in contrast to the taphonomic disparity seen in the Phanerozoic fossil record, where most fossils are skeletal and Lagerstätten such as the Chengjiang biota can have a prominent effect (fig. S7C). Thus, while the Proterozoic fossil record is poor, perhaps it is more or less uniformly poor throughout

the entire eon. If so, the richness pattern revealed in our fossil diversity curve is informative. Nonetheless, we emphasize that the focus of this study is eukaryotic fossil diversity, which is the only available proxy for the diversity of early eukaryotes.

Discussion

A Cryogenian divide

The quantitative results indicate that global glaciations played a first-order control on the macroevolution of Proterozoic eukaryotes. The evolutionary patterns and dynamics of Proterozoic eukaryotes are markedly different before and after Cryogenian glaciations (Figs. 1A and 2). The differences are highlighted by the notably low fossil diversity, origination rates, and extinction rates before the Cryogenian relative to those after, quantitatively confirming previous suggestions that Cryogenian glaciations served as a major divide in the macroevolution of early eukaryotes (*24*, *40*). This first-order pattern is also consistent with biomarker data and morphological disparity of Proterozoic eukaryotes (*13*, *41*), which point to a profound ecological revolution of primary producers in the late Cryogenian Period (*41*) and a substantial expansion of eukaryotic morphospace in the Ediacaran (*13*, *42*). Within the Ediacaran Period, a secondary divide is the Gaskiers glaciation, which was probably a regional event (*27*) but was associated with major decline in eukaryotic fossil diversity and ushered in much greater origination and extinction rates (Fig. 3, A to C).

Other Proterozoic tectonic, environmental, and ecological events (*43*) may have also temporally coupled with the evolutionary tempo of early eukaryotes (Fig. 4), although the temporal resolution of these events is still poor, preventing their precise correlation with biodiversity events and exploration of causal relationships. Nonetheless, our quantitative analysis confirms a possible correlation of the Mesoproterozoic stasis of eukaryote biodiversity (Fig. 4H) with the formation of the Rodinia supercontinent (Fig. 4A), stable atmospheric pO_2 (partial pressure of oxygen) levels (Fig. 4B), largely invariant carbonate carbon isotope ($\delta^{13}C_{carb}$) values (Fig. 4C), relatively low [Mo] in fine-grained sediments (Fig. 4D), scarcity of large phosphorite deposits (Fig. 4E), atmospheric and oceanic redox proxies (e.g., Fig. 4F), and the dominance of phototrophic bacterial biomarkers (Fig. 4G). Such coordinated stasis of multiple proxies suggests that the Earth system may have been at a long-term equilibrium (*26*), despite the appearance of evolutionary novelties in this time period (Fig. 4H). In contrast, all these proxies show large-scale variations after the "Boring Billion" and particularly in the Ediacaran and early Cambrian periods (Fig. 4), suggesting stronger perturbations to the Earth system.

The "Boring Billion"

The fossil species diversity pattern provides valuable perspectives on the evolutionary trajectory of eukaryotes during the "Boring Billion" (~1.8 to 0.8 billion years ago). It has long been argued that the "Boring Billion" is distinguished by a prolonged evolutionary stasis (*12*, *25*), which may have been coupled with stability in $\delta^{13}C_{carb}$ (*9*, *25*), crustal dynamics (*43*), redox state of surface environments (*9*), and planetary climate (*44*) (Fig. 4, A to F). However, recent paleontological, molecular clock, and geobiological advances suggest that complex eukaryotes may have a deep root in the "Boring Billion" (*45*) (Fig. 4, G and H). For example, an array of multicellular macrofossils have been discovered during this interval, including the earliest multicellular red and green algae at ~1 billion years ago (*19*, *46*). Consistent with these paleontological records, recent molecular clock analyses show that major eukaryotic clades diverged during the "Boring Billion," although these predictions usually come with large error bars (*47*, *48*). In addition, a recent biomarker analysis indicates that stem-group eukaryotes may have a deep root in the Mesoproterozoic (*41*). Thus, multiple independent lines of evidence suggest that important evolutionary events of eukaryotes occurred in the "Boring Billion" (*45*). It is important to point out, however, that evolutionary innovations and phylogenetic divergences do not necessarily translate into taxonomic diversity and ecological impact on the Earth system unless they are scaled up globally. Thus, the low fossil diversity documented in this paper (Fig. 1A), as well as the limited ecological abundance and morphological disparity of eukaryotes in the "Boring Billion" relative to the Ediacaran and Cambrian periods (*13*, *41*), can be reconciled with Mesoproterozoic evolution of important eukaryote clades by invoking a long delay from phylogenetic divergence to ecologic and taxonomic dominance (*24*, *49*).

The Cryogenian biosphere

The CONOP results shed new light on the biological response to Cryogenian glaciations (*10*). Regardless of whether the two Cryogenian glaciations (i.e., the Sturtian and Marinoan glaciations) represent hard or soft Snowball Earth (*50*), they would have had a strong impact on the biosphere, particularly eukaryotic life, which managed to survive these glaciations (*51*). The investigation of biological response to the Snowball Earth events, however, is hampered by the dearth of Cryogenian fossils. There are so far only 24 named eukaryotic species reported from Cryogenian sediments, along with several unnamed eukaryotic taxa and additional bacterial microfossil taxa (*20*, *36*, *52*) (table S1). The CONOP analysis shows that, in addition to the fossils reported from the Cryogenian sediments, 53 additional eukaryotic species ranged through and thus survived the Cryogenian glaciations (table S1). These species belong to several groups of eukaryotes, including the spiny acritarchs *Cymatiosphaeroides kullingii*, *Eotylotopalla delicata*, *Caudosphaera expansa*, and *Germinosphaera* sp.; and the multicellular or coenocytic eukaryotes *Horodyskia minor*, *H. moniliformis*, *Parmia anastassiae*, and *Jacutianema solubila* [see the supplementary text in the supplementary materials (*29*)]. Although these are necessarily morphospecies, they have relatively complex morphologies that facilitate taxonomic identification and are less likely to represent evolutionary convergence. Hence, the Cryogenian biosphere probably comprised heterotrophic eukaryotes, benthic macroalgae, planktonic microalgae, and photosynthetic bacteria, some of which must have survived the Cryogenian glaciations. This conclusion is further supported by the evolutionary continuity of suprageneric groups, such as red and green algae, whose fossils are found both before and after the Cryogenian Period (*19*, *41*, *46*). Further evidence for the survival of red algae is offered by the presence of their biomarkers before and after the Cryogenian (*41*).

Ediacaran evolutionary dynamics

The accelerated evolutionary dynamics in the Ediacaran Period is exemplified by the rapid decline in fossil diversity starting at the Gaskiers glaciation, representing the earliest mass extinction of eukaryotes documented in the Proterozoic. This extinction was mainly driven by the rapid disappearance of Doushantuo-Pertatataka acritarchs (DPAs, morphologically complex organic-walled microfossils conventionally interpreted as unicellular eukaryotes), resulting in the disappearance of 70% of fossil species between 581 and 573 Ma (Figs. 1 and 3A). Although several previous studies argued that some DPAs may have extended to the late Ediacaran (*53*, *54*), their diversity is exceedingly low (*55*). It is unlikely that this extinction is a preservational artifact, because phosphorites, chert nodules, and mudstones or shales, which archive early Ediacaran diversity of DPAs, are also known in the late Ediacaran but preserve few or no DPAs [e.g., (*56*)].

The triggers for the DPA extinction event remain obscure. Some have proposed that the ventilation of deep oceans during the Shuram excursion ~574 to 567 Ma (*57*, *58*) and the ecological expansion of animals may have played key roles in driving DPA disappearance (*59*). However, our analysis showed that the onset of this extinction at ~581 Ma predated the Shuram excursion and the first appearance of macroscopic animal fossils (*57*) (Fig. 3E) but was temporally coupled with the Gaskiers glaciation (*27*) (Figs. 1, A and C, and 3E), consistent with the hypothesis that global cooling could have been a trigger for DPA extinction (*59*).

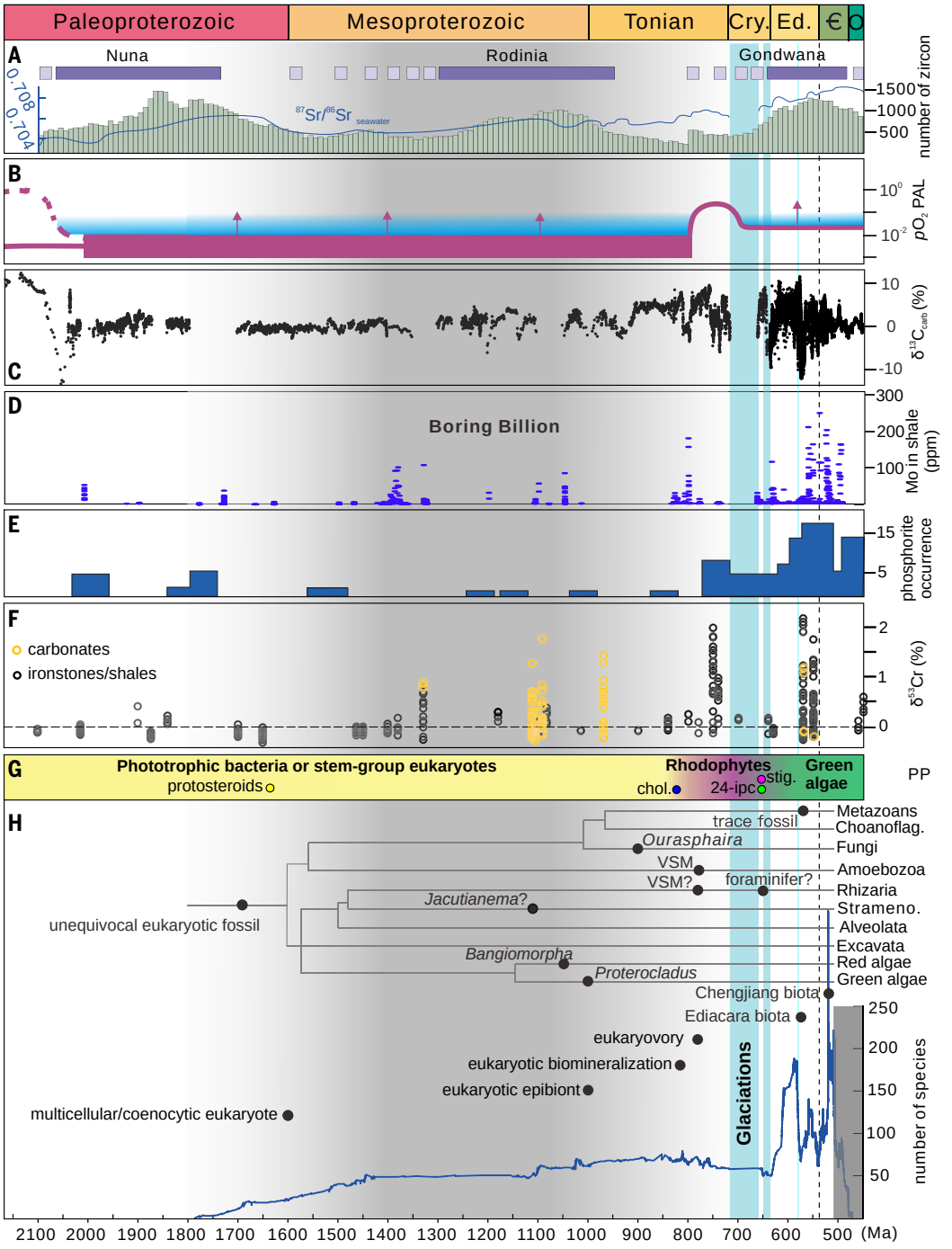

Fig. 4. Proterozoic evolutionary, environmental, ecological, and tectonic events and trends. (**A**) Super- and megacontinent cycles, detrital zircon abundance, and $^{87}Sr/^{86}Sr$ ratios (*74*). Solid dark-purple bars represent duration of supercontinents, and spaced light-purple squares denote assembly or rifting of supercontinents. (**B**) Schematic diagram showing the evolution of atmospheric pO_2 levels (*9*). Arrows denote possible transient increases in pO_2. Red color represents pO_2 estimates based on proxy data, and blue color represents alternative estimates based on numerical simulations that predict O_2 stability at higher pO_2 levels (*9*). PAL, present atmospheric level. (**C**) $\delta^{13}C_{carb}$ data (*57*, *73*). (**D**) Mo concentrations in euxinic shales (*75*). ppm, parts per million. (**E**) Sedimentary phosphorite occurrences (*76*). (**F**) $\delta^{53}Cr$ values (*77*). (**G**) Ecological transition of dominant primary producers (PP) denoted by color shades, and the first known record of major lipids marked by circles (*41*). chol., cholesteroids; 24-ipc, 24-isopropylcholestane; stig., stigmasteroids. (**H**) The earliest known fossil records of major eukaryotic groups mapped on a time-calibrated phylogenetic tree, biodiversity of Proterozoic eukaryotic fossils (from Fig. 1A), and major evolutionary innovations, modified from (*45*). Question marks denote tentative phylogenetic placements of the microfossils. See Table 1 for reference details of the fossil assignments. Vertical bars and abbreviations are the same as in Fig. 1. Choanoflag., choanoflagellates; Strameno., stramenopiles; VSM, vase-shaped microfossil.

Our study provides important constraints on the evolutionary tempo of early animals. There has been considerable debate on molecular clock estimates of metazoan divergence time (*60*, *61*), which necessarily predates the ecological expansion and taxonomic diversification of animals documented in the fossil record. The diversification of Ediacara-type macrofossils, most of which have been interpreted as stem-group and even crown-group animals (*62*), and the appearance of animal trace fossils soon after the extinction of DPAs opened a new chapter of Ediacaran eukaryotic evolution, one characterized by the rise of macroscopic animals. This evolutionary event coincides with the nadir of the Shuram excursion (Fig. 3), an event proposed to have been driven by deep ocean ventilation [(*58*, *63*), but see (*64*)]. This temporal association is consistent with a possible causal relationship between oceanic oxygenation and the rise of macroscopic animals, as has been previously suggested (*65*).

The CONOP results also provide quantitative insights into the evolutionary tempo of

Table 1. The earliest known fossil occurrences of major eukaryotic lineages and evolutionary innovations shown in Fig. 4H.

Lineages or evolutionary events	Fossils or biomarkers	Age (Ma)	Reference
Fungi	*Ourasphaira*	1013–892	(*78*)
Green algae (Chlorophyta)	*Proterocladus*	~1000	(*19*)
Rhodophyta	*Bangiomorpha*	1047	(*46*, *79*)
Rhizaria	Tests of possible foraminifera	659–645	(*10*, *80*)
	Vase-shaped microfossil *Melicerion*	789–729	(*81*)
Amoebozoa	Vase-shaped microfossils	789–729	(*81*, *82*)
Stramenopiles	*Jacutianema*	>1109	(*83*)
Metazoans	Ediacara biota (*29*)	574	(*65*)
	Trace fossils	574	(*65*)
	Chengjiang biota	~520	(*84*)
Eukaryovory	Perforation on organic-walled microfossils	1013–892	(*85*)
Eukaryotic epibionts	Dark discoid structures on *Tawuia*	1000	(*86*)
Eukaryotic biomineralization	Apatitic-scale microfossils	~810	(*87*)
Multicellular or coenocytic eukaryote	*Tawuia*	~1600	(*88*)

the three assemblages of Ediacara-type macrofossils, that is, the Avalon (~575 to 560 Ma), White Sea (~560 to 550 Ma), and Nama (~550 to 539 Ma) assemblages (Figs. 1C and 3A). Previous attempts to estimate the diversity of Ediacara-type macrofossils were based on genus-level occurrence data binned in the three abovementioned assemblages (*42*, *66*), necessarily with coarse temporal resolution. In contrast, the CONOP computation reported here was built on species-level data with more thorough assessment of sampling biases and much better temporal resolution. The CONOP results show that the first decline in the diversity of Ediacara-type macrofossils occurred by the end of the White Sea interval (~551 Ma), with a 51% drop in species richness in 0.7 ± 1.1 Myr, followed by another drop of 79% near the Precambrian-Cambrian boundary (~542 to 539 Ma). Together, these two events resulted in an 85% loss of total species richness since the White Sea interval and represent the first two documented mass extinctions in the history of animals (*66*). Finally, the CONOP results show a strong correlation in fossil species richness between total eukaryotes and animals in the late Ediacaran, with other eukaryotic fossils remaining relatively stable in species richness (Fig. 3A), indicating that Ediacaran animals (mostly represented by Ediacara-type macrofossils) contributed to eukaryote diversity but did not drive diversification of nonanimal eukaryote diversity through positive ecological interactions. In contrast, fossil species richness of animals and unicellular eukaryotes increased in tandem in the early Cambrian, indicating that Cambrian animals may have accelerated the diversification of nonanimal eukaryotes through positive ecological interactions such as grazing and predation (*40*) and highlighting the ecological differences between Ediacaran and Cambrian faunas.

Materials and methods summary

The following is a brief summary of the materials and methods. Please see the full materials and methods in the supplementary materials for more details.

Data compilation and filtering

The database comprises Proterozoic–Cambrian paleontological, geochronological, lithostratigraphic, and geochemical data acquired from the literature up to July 2023 [figs. S1 to S3; data S1 (*23*)], supplemented with additional Cambrian and Ordovician data from OneStratigraphy (http://onestratigraphy.ddeworld.org). Key radiometric ages, sedimentological marker beds, geochemical excursions, and fossil occurrences with convincingly eukaryotic affinity were included in our dataset along with their stratigraphic depth information in each section. To avoid inflation of species richness, synonyms, ontogenetic variations, and taphonomic alterations were carefully examined. Published taxa with taxonomic identifications only above the genus level were excluded from the dataset. Species in open nomenclature were generally excluded, although some open nomenclatures of Ediacara-type macrofossils and acritarchs, which were often reported only at the genus level or as open nomenclatures, were assessed on a case-by-case basis. Species were tagged as "likely eukaryotes" and "possible eukaryotes," which were used in sensitivity tests for uncertainty in phylogenetic interpretations. Additionally, a network analysis was conducted to detect isolated sections or cluster of sections that shared no taxa with others. These sections were excluded from the dataset and CONOP analysis as they provide no useful information to inter-section correlation (fig. S3). Finally, the time interval after Cambrian Age 4 (i.e., <509 Ma) was treated as a buffer zone owing to incomplete biostratigraphic data, which induces edge effects of the dataset (*17*, *67*).

CONOP computation

CONOP was used to optimize correlations across all studied sections and to develop the best-fit composite sequence for all studied species. Given that our dataset comprises hundreds of sections, representing various sampling intensity and sedimentary rates, the "level" option was used in the CONOP computation so that the calculation was conducted on the basis of sampling levels. More methodological details of CONOP analysis and unbinned richness calculation have been thoroughly described in previous publications (*2*, *6*, *22*).

To test the stability of the CONOP solution and the robustness of the fossil species diversity pattern, multiple independent CONOP runs were conducted using the full dataset (fig. S6A). Additionally, we conducted an independent CONOP run using a culled dataset with all open nomenclatures excluded (fig. S7A, yellow curve) to test whether the inclusion of open nomenclatures or ambiguous species identifications (such as xx sp., xx sp. A, xx sp. B, etc.) in our dataset would systematically bias the results of species diversity pattern. This sensitivity test was supplemented by a post-CONOP sensitivity test, in which the open nomenclatures were removed from the best-fit composite sequence (Fig. 1A) to generate a new richness curve (fig. S7A, green curve).

Fossil groups

For convenience of communication, all eukaryotic taxa in our dataset were divided into four major groups: (i) unicellular eukaryotes that consist of single-celled eukaryotes of microscopic size; (ii) multicellular or coenocytic eukaryotes that are composed of multicellular and large unicellular eukaryotes presumably with multiple nuclei; (iii) animal body fossils that include the majority of Ediacara-type macrofossils and tubular fossils; and (iv) animal trace fossils.

In addition, to test the potential impact of phylogenetically equivocal taxa on the eukaryotic fossil diversity patterns, all fossil taxa in our dataset were tagged as likely eukaryotes or possible eukaryotes [data S1 (*23*)], and a sensitivity test was conducted by excluding "possible eukaryotes" from the best-fit composite sequence (Fig. 1A), resulting in a new fossil species diversity curve (fig. S7B). In this way, the potential influence of phylogenetically equivocal taxa on the fossil diversity curve could be

assessed by a comparison between the total and culled richness curves (fig. S7B).

Age constraints and models

The ordination of fossil events in CONOP computation was supplemented and time-calibrated by additions of associated radiometric ages, sedimentological marker beds, and $\delta^{13}C_{carb}$ excursions. Given that Cambrian sequences are generally well constrained by biozones (*68*), we also used Cambrian biozonal species, in addition to the above-mentioned proxies, for age constraints. Ultimately, a total of 35 biozonal species in their globally recognized chronostratigraphic order (*68*) were chosen to constrain the timeline for Cambrian events (fig. S10).

To construct an age model that takes into consideration the uncertainty of radiometric ages, we applied Bchron Bayesian interpolation statistics to build a probabilistic age-depth model based on the radiometric ages, their uncertainties, and their associated stratigraphic position in the composite sequence of the optimal CONOP solution (Fig. 1A), as per the algorithm of Haslett and Parnell (*69*). The age-depth model was conducted using R package Bchron (http://cran.r-project.org/web/packages/Bchron/index.html), which predicted the age and its associated 95% confidence interval for each temporal level in the composite sequence (Fig. 1A and fig. S9).

Statistical test on sampling bias

There are three major sources of sampling bias in our study: sampling incompleteness due to incomplete fossil preservation and sampling, uneven fossil sampling among different sections and among different time intervals, and uneven supporting sections or sequences between different time intervals. To evaluate these biases, we carried out the following three statistical tests, with singletons (whose FAD and LAD are in the same temporal level) excluded from these analyses. (i) To test the potential influence of sampling biases, 1000 iterations of bootstrap analyses were conducted on the basis of the best-fit composite sequence from the CONOP analysis. A 95% confidence interval was generated from the bootstrap analysis to illustrate the robustness of richness patterns (Fig. 1A). (ii) To evaluate the influence of uneven fossil sampling intensity among geological intervals, 1000 iterations of rarefaction analyses were applied to nonsingleton species at local sections scaled to the CONOP result, following methods described in (*70*) (fig. S6B). (iii) To evaluate the influence of variable section numbers in different time intervals, a 10-Myr sliding bin calculation technique was used to generate a standardized or normalized diversity curve (fig. S6C). Technical details of bootstrapping, rarefaction, and standardization are described in the materials and methods section of the supplementary materials and in previous publications (*2*, *6*).

In addition, to test whether Lagerstätten (e.g., the Chengjiang biota, which tends to contain a large number of taxa with short stratigraphic ranges) may have biased the richness patterns of eukaryotic fossils, a new fossil diversity construction (fig. S7C) was conducted by excluding short-ranging taxa (<0.1 Myr) from the best-fit CONOP composite sequence underlying Fig. 1A. Also, to test whether the uneven availability of sedimentary rocks through time may have affected the diversity pattern of early eukaryotic fossils, a comparison has been made between the fossil diversity and rock availability during the study interval. Two rock databases were used for this purpose: Macrostrat (https://macrostrat.org) and the published database of Ronov (*71*).

Species diversity dynamics

An array of diversity dynamic metrics were calculated on the basis of the best-fit composite sequence constructed by CONOP computation, including rates of origination, extinction, proportional origination, proportional extinction, proportional diversification, proportional turnover, mean species longevity, and species/genus ratio on a controlled uniform time bin (Figs. 2 and 3 and figs. S4 and S5). These metrics were calculated following Deng *et al.* (*6*). Briefly, the origination and extinction rates were calculated from the number of new species (N_o) and extinct species (N_e) in each of a series of time bins. The results are reported as the number of species per bin. The proportional origination (P_o) and extinction (P_e) rates were calculated by dividing the N_o and N_e by the total number of species in the corresponding time bin and reported as fraction per bin. The proportional diversification (P_d) and turnover (P_t) rates were assessed using the following equations: $P_d = P_o - P_e$; $P_t = P_o + P_e$. In addition, three types of mean longevity were estimated on the basis of the best-fit composite sequence, including mean longevity of total, new, and extinct species at each temporal level (*72*). The longevity of each species $L = AgeF - AgeL$, where $AgeF$ and $AgeL$ represent the age of the first and last appearances, respectively. The mean longevity represents an aggregation comprising the mean longevity of the cohort of species in each temporal level. For the mean longevity of new taxa (or extinct taxa), only the species that originated (or went extinct) at the respective temporal level were used in the calculation. Calculation of these metrics was repeated with "possible eukaryotes" excluded (fig. S4). Finally, the species/genus ratio was generated by using the genus richness to divide the species richness at each temporal level (Fig. 2F).

REFERENCES AND NOTES

1. D. M. Raup, J. J. Sepkoski Jr., Mass extinctions in the marine fossil record. *Science* **215**, 1501–1503 (1982). doi: 10.1126/science.215.4539.1501; pmid: 17788674
2. J. X. Fan *et al.*, A high-resolution summary of Cambrian to Early Triassic marine invertebrate biodiversity. *Science* **367**, 272–277 (2020). doi: 10.1126/science.aax4953; pmid: 31949075
3. B. Hannisdal, S. E. Peters, Phanerozoic Earth system evolution and marine biodiversity. *Science* **334**, 1121–1124 (2011). doi: 10.1126/science.1210695; pmid: 22116884
4. S. Z. Shen *et al.*, Calibrating the end-Permian mass extinction. *Science* **334**, 1367–1372 (2011). doi: 10.1126/science.1213454; pmid: 22096103
5. B. Schoene *et al.*, U-Pb constraints on pulsed eruption of the Deccan Traps across the end-Cretaceous mass extinction. *Science* **363**, 862–866 (2019). doi: 10.1126/science.aau2422; pmid: 30792300
6. Y. Y. Deng *et al.*, Timing and patterns of the Great Ordovician Biodiversification Event and Late Ordovician mass extinction: Perspectives from South China. *Earth Sci. Rev.* **220**, 103743 (2021). doi: 10.1016/j.earscirev.2021.103743
7. C. R. Marshall, Forty years later: The status of the "Big Five" mass extinctions. *Camb. Prism. Extinct.* **1**, e5 (2023). doi: 10.1017/ext.2022.4
8. Z.-X. Li, Y. Liu, R. Ernst, A dynamic 2000–540 Ma Earth history: From cratonic amalgamation to the age of supercontinent cycle. *Earth Sci. Rev.* **238**, 104336 (2023). doi: 10.1016/j.earscirev.2023.104336
9. T. W. Lyons, C. W. Diamond, N. J. Planavsky, C. T. Reinhard, C. Li, Oxygenation, life, and the planetary system during Earth's middle history: An overview. *Astrobiology* **21**, 906–923 (2021). doi: 10.1089/ast.2020.2418; pmid: 34314605
10. P. F. Hoffman *et al.*, Snowball Earth climate dynamics and Cryogenian geology-geobiology. *Sci. Adv.* **3**, e1600983 (2017). doi: 10.1126/sciadv.1600983; pmid: 29134193
11. G. Vidal, M. Moczydłowska-Vidal, Biodiversity, speciation, and extinction trends of Proterozoic and Cambrian phytoplankton. *Paleobiology* **23**, 230–246 (1997). doi: 10.1017/S0094837300016808
12. A. H. Knoll, Proterozoic and early Cambrian protists: Evidence for accelerating evolutionary tempo. *Proc. Natl. Acad. Sci. U.S.A.* **91**, 6743–6750 (1994). doi: 10.1073/pnas.91.15.6743; pmid: 8041692
13. N. Bykova *et al.*, Seaweeds through time: Morphological and ecological analysis of Proterozoic and early Paleozoic benthic macroalgae. *Precambrian Res.* **350**, 105875 (2020). doi: 10.1016/j.precamres.2020.105875
14. J. W. Huntley, S. Xiao, M. Kowalewski, 1.3 billion years of acritarch history: An empirical morphospace approach. *Precambrian Res.* **144**, 52–68 (2006). doi: 10.1016/j.precamres.2005.11.003
15. P. A. Cohen, F. A. Macdonald, The Proterozoic record of eukaryotes. *Paleobiology* **41**, 610–632 (2015). doi: 10.1017/pab.2015.25
16. A. H. Knoll, E. J. Javaux, D. Hewitt, P. Cohen, Eukaryotic organisms in Proterozoic oceans. *Philos. Trans. R. Soc. Lond. B Biol. Sci.* **361**, 1023–1038 (2006). doi: 10.1098/rstb.2006.1843; pmid: 16754612
17. L. A. Riedman, P. M. Sadler, Global species richness record and biostratigraphic potential of early to middle Neoproterozoic eukaryote fossils. *Precambrian Res.* **319**, 6–18 (2018). doi: 10.1016/j.precamres.2017.10.008
18. P. Liu, M. Moczydłowska, Ediacaran microfossils from the Doushantuo Formation chert nodules in the Yangtze Gorges area, South China, and new biozones. *Fossils Strata* **65**, 1–172 (2019). doi: 10.1002/9781119564225.ch1
19. Q. Tang, K. Pang, X. Yuan, S. Xiao, A one-billion-year-old multicellular chlorophyte. *Nat. Ecol. Evol.* **4**, 543–549 (2020). doi: 10.1038/s41559-020-1122-9; pmid: 32094536
20. Q. Ye *et al.*, The survival of benthic macroscopic phototrophs on a Neoproterozoic snowball Earth. *Geology* **43**, 507–510 (2015). doi: 10.1130/G36640.1
21. P. M. Sadler, R. A. Cooper, M. Melchin, High-resolution, early Paleozoic (Ordovician-Silurian) time scales. *Geol. Soc. Am. Bull.* **121**, 887–906 (2009). doi: 10.1130/B26357.1
22. P. Sadler, "Biochronology as a Traveling Salesman Problem: Introduction to the CONOP9 Seriation Programs" (Dept. of Earth Sciences, Univ. of California, Riverside, 2013).
23. Q. Tang *et al.*, Quantifying the global biodiversity of Proterozoic eukaryotes, Dryad (2024); https://doi.org/10.5061/dryad.8w9ghx3w6.
24. N. J. Butterfield, Macroevolution and macroecology through deep time. *Palaeontology* **50**, 41–55 (2007). doi: 10.1111/j.1475-4983.2006.00613.x
25. R. Buick, D. J. Des Marais, A. H. Knoll, Stable isotopic compositions of carbonates from the Mesoproterozoic

Bangemall Group, northwestern Australia. *Chem. Geol.* **123**, 153–171 (1995). doi: 10.1016/0009-2541(95)00049-R; pmid: 11540130
26. R. Mitchell, D. A. Evans, The Balanced Billion. *GSA Today* **34**, 10–11 (2024). doi: 10.1130/GSATG423C.1
27. J. P. Pu *et al*., Dodging snowballs: Geochronology of the Gaskiers glaciation and the first appearance of the Ediacaran biota. *Geology* **44**, 955–958 (2016). doi: 10.1130/G38284.1
28. J. W. Valentine, *On the Origin of Phyla* (Univ. of Chicago Press, 2004).
29. The supplementary materials include materials and methods, supplementary text, supplementary figures, and a supplementary table.
30. D. C. Segessenman, S. E. Peters, Transgression–regression cycles drive correlations in Ediacaran–Cambrian rock and fossil records. *Paleobiology* **50**, 150–163 (2024). doi: 10.1017/pab.2023.31
31. S. Zhang *et al*., Orbital forcing of climate 1.4 billion years ago. *Proc. Natl. Acad. Sci. U.S.A.* **112**, E1406–E1413 (2015). doi: 10.1073/pnas.1502239112; pmid: 25775605
32. X. Lang *et al*., Cracking the superheavy pyrite enigma: Possible roles of volatile organosulfur compound emission. *Natl. Sci. Rev.* **8**, nwab034 (2021). doi: 10.1093/nsr/nwab034; pmid: 34858606
33. K. Grey, A. C. Hill, C. Calver, "Biostratigraphy and stratigraphic subdivision of Cryogenian successions of Australia in a global context" in *The Geological Record of Neoproterozoic Glaciations*, vol. 36 of *The Geological Society of London Memoirs*, E. Arnaud, G. P. Halverson, G. Shields-Zhou, Eds. (The Geological Society of London, 2011), pp. 113–134.
34. K. Pang *et al*., Integrated Meso-Neoproterozoic stratigraphy in the Jiao-Liao-Xu-Huai area of North China Craton: A review. *Dicengxue Zazhi* **45**, 467–492 (2021). doi: 10.19839/j.cnki.dcxzz.2021.0019
35. L. Miao, M. Moczydłowska, M. Zhu, A diverse organic-walled microfossil assemblage from the Mesoproterozoic Xiamaling Formation, North China. *Precambrian Res.* **360**, 106235 (2021). doi: 10.1016/j.precamres.2021.106235
36. L. A. Riedman, S. M. Porter, G. P. Halverson, M. T. Hurtgen, C. K. Junium, Organic-walled microfossil assemblages from glacial and interglacial Neoproterozoic units of Australia and Svalbard. *Geology* **42**, 1011–1014 (2014). doi: 10.1130/G35901.1
37. L. A. Riedman, S. Porter, Organic-walled microfossils of the mid-Neoproterozoic Alinya Formation, Officer Basin, Australia. *J. Paleontol.* **90**, 854–887 (2016). doi: 10.1017/jpa.2016.49
38. C. Dehler *et al*., Synthesis of the 780–740 Ma Chuar, Uinta Mountain, and Pahrump (ChUMP) groups, western USA: Implications for Laurentia-wide cratonic marine basins. *Geol. Soc. Am. Bull.* **129**, 607–624 (2017). doi: 10.1130/B31532.1
39. W. Zheng *et al*., The Proterozoic Qinggouzi microfossil assemblage and its biostratigraphic constraints on the Great Unconformity in northeastern North China Craton. *Precambrian Res.* **395**, 107130 (2023). doi: 10.1016/j.precamres.2023.107130
40. K. J. Peterson, N. J. Butterfield, Origin of the Eumetazoa: Testing ecological predictions of molecular clocks against the Proterozoic fossil record. *Proc. Natl. Acad. Sci. U.S.A.* **102**, 9547–9552 (2005). doi: 10.1073/pnas.0503660102; pmid: 15983372
41. J. J. Brocks *et al*., Lost world of complex life and the late rise of the eukaryotic crown. *Nature* **618**, 767–773 (2023). doi: 10.1038/s41586-023-06170-w; pmid: 37286610
42. B. Shen, L. Dong, S. Xiao, M. Kowalewski, The Avalon explosion: Evolution of Ediacara morphospace. *Science* **319**, 81–84 (2008). doi: 10.1126/science.1150279; pmid: 18174439
43. M. Tang, X. Chu, J. Hao, B. Shen, Orogenic quiescence in Earth's middle age. *Science* **371**, 728–731 (2021). doi: 10.1126/science.abf1876; pmid: 33574211
44. M. D. Brasier, J. F. Lindsay, A billion years of environmental stability and the emergence of eukaryotes: New data from northern Australia. *Geology* **26**, 555–558 (1998). doi: 10.1130/0091-7613(1998)026<0555:ABYOES>2.3.CO;2; pmid: 11541449
45. X. Yuan *et al*., The origin and early evolution of complex organisms. *Kexue Tongbao* **68**, 169–187 (2023). doi: 10.1360/TB-2022-0804
46. N. J. Butterfield, *Bangiomorpha pubescens* n. gen., n. sp.: Implications for the evolution of sex, multicellularity, and the Mesoproterozoic-Neoproterozoic radiation of eukaryotes. *Paleobiology* **26**, 386–404 (2000). doi: 10.1666/0094-8373(2000)026<0386:BPNGNS>2.0.CO;2
47. J. F. H. Strassert, I. Irisarri, T. A. Williams, F. Burki, A molecular timescale for eukaryote evolution with implications for the origin of red algal-derived plastids. *Nat. Commun.* **12**, 1879 (2021). doi: 10.1038/s41467-021-22044-z; pmid: 33767194
48. Z. Hou *et al*., Phylotranscriptomic insights into a Mesoproterozoic-Neoproterozoic origin and early radiation of green seaweeds (Ulvophyceae). *Nat. Commun.* **13**, 1610 (2022). doi: 10.1038/s41467-022-29282-9; pmid: 35318329
49. S. M. Porter, Insights into eukaryogenesis from the fossil record. *Interface Focus* **10**, 20190105 (2020). doi: 10.1098/rsfs.2019.0105; pmid: 32642050
50. T. Bechstädt *et al*., The Cryogenian Ghaub Formation of Namibia – New insights into Neoproterozoic glaciations. *Earth Sci. Rev.* **177**, 678–714 (2018). doi: 10.1016/j.earscirev.2017.11.028
51. H. Song *et al*., Mid-latitudinal habitable environment for marine eukaryotes during the waning stage of the Marinoan snowball glaciation. *Nat. Commun.* **14**, 1564 (2023). doi: 10.1038/s41467-023-37172-x; pmid: 37015913
52. L. Morais *et al*., Diverse vase-shaped microfossils within a Cryogenian glacial setting in the Urucum Formation (Brazil). *Precambrian Res.* **367**, 106470 (2021). doi: 10.1016/j.precamres.2021.106470
53. D. Grazhdankin *et al*., Doushantuo-Pertatataka–type acanthomorphs and Ediacaran ecosystem stability. *Geology* **48**, 708–712 (2020). doi: 10.1130/G47467.1
54. R. P. Anderson, F. A. Macdonald, D. S. Jones, S. McMahon, D. E. G. Briggs, Doushantuo-type microfossils from latest Ediacaran phosphorites of northern Mongolia. *Geology* **45**, 1079–1082 (2017). doi: 10.1130/G39576.1
55. S. Xiao *et al*., Systematic paleontology, acritarch biostratigraphy, and $\delta^{13}C$ chemostratigraphy of the early Ediacaran Krol A Formation, Lesser Himalaya, northern India. *J. Paleontol.* **98**, 159–220 (2024). doi: 10.1017/jpa.2022.7
56. Q. Ye *et al*., Phosphatized microfossils from the Miaohe Member of South China and their implications for the terminal Ediacaran biodiversity decline. *Precambrian Res.* **388**, 107001 (2023). doi: 10.1016/j.precamres.2023.107001
57. C. Yang *et al*., The tempo of Ediacaran evolution. *Sci. Adv.* **7**, eabi9643 (2021). doi: 10.1126/sciadv.abi9643; pmid: 34731004
58. D. T. Johnston *et al*., Late Ediacaran redox stability and metazoan evolution. *Earth Planet. Sci. Lett.* **335–336**, 25–35 (2012). doi: 10.1016/j.epsl.2012.05.010
59. C. Zhou, G. Xie, K. McFadden, S. Xiao, X. Yuan, The diversification and extinction of Doushantuo-Pertatataka acritarchs in South China: Causes and biostratigraphic significance. *Geol. J.* **42**, 229–262 (2007). doi: 10.1002/gj.1062
60. G. E. Budd, R. P. Mann, Survival and selection biases in early animal evolution and a source of systematic overestimation in molecular clocks. *Interface Focus* **10**, 20190110 (2020). doi: 10.1098/rsfs.2019.0110; pmid: 32637066
61. M. dos Reis *et al*., Uncertainty in the timing of origin of animals and the limits of precision in molecular timescales. *Curr. Biol.* **25**, 2939–2950 (2015). doi: 10.1016/j.cub.2015.09.066; pmid: 26603774
62. S. Xiao, M. Laflamme, On the eve of animal radiation: Phylogeny, ecology and evolution of the Ediacara biota. *Trends Ecol. Evol.* **24**, 31–40 (2009). doi: 10.1016/j.tree.2008.07.015; pmid: 18952316
63. D. A. Fike, J. P. Grotzinger, L. M. Pratt, R. E. Summons, Oxidation of the Ediacaran ocean. *Nature* **444**, 744–747 (2006). doi: 10.1038/nature05345; pmid: 17151665
64. E. A. Sperling *et al*., Statistical analysis of iron geochemical data suggests limited late Proterozoic oxygenation. *Nature* **523**, 451–454 (2015). doi: 10.1038/nature14589; pmid: 26201598
65. A. D. Rooney *et al*., Calibrating the coevolution of Ediacaran life and environment. *Proc. Natl. Acad. Sci. U.S.A.* **117**, 16824–16830 (2020). doi: 10.1073/pnas.2002918117; pmid: 32632000
66. S. A. F. Darroch, E. F. Smith, M. Laflamme, D. H. Erwin, Ediacaran extinction and Cambrian explosion. *Trends Ecol. Evol.* **33**, 653–663 (2018). doi: 10.1016/j.tree.2018.06.003; pmid: 30007844
67. M. Foote, Origination and extinction components of taxonomic diversity: General problems. *Paleobiology* **26**, 74–102 (2000). doi: 10.1666/0094-8373(2000)26[74:OAECOT]2.0.CO;2
68. S. C. Peng, L. E. Babcock, P. Ahlberg, "The Cambrian Period" in *Geologic Time Scale 2020, Volume 2, Part IV: Geologic Periods: Phanerozoic*, F. M. Gradstein, J. G. Ogg, M. D. Schmitz, G. M. Ogg, Eds. (Elsevier, 2020), pp. 565–629. doi: 10.1016/B978-0-12-824360-2.00019-X
69. J. Haslett, A. Parnell, A simple monotone process with application to radiocarbon-dated depth chronologies. *J. R. Stat. Soc. Ser. C Appl. Stat.* **57**, 399–418 (2008). doi: 10.1111/j.1467-9876.2008.00623.x
70. Y. Wang *et al*., Quantifying the process and abruptness of the end-Permian mass extinction. *Paleobiology* **40**, 113–129 (2014). doi: 10.1666/13022
71. A. B. Ronov, The Earth's sedimentary shell (quantitative patterns of its structure, compositions, and evolution). *Int. Geol. Rev.* **24**, 1313–1363 (1982). doi: 10.1080/00206818209451075
72. Y. Deng *et al*., No Furongian Biodiversity Gap: Evidence from South China. *Palaeogeogr. Palaeoclimatol. Palaeoecol.* **618**, 111492 (2023). doi: 10.1016/j.palaeo.2023.111492
73. B. D. Cramer, I. Jarvis, "Carbon isotope stratigraphy" in *Geologic Time Scale 2020, Volume 1, Part I: Introduction*, F. M. Gradstein, J. G. Ogg, M. D. Schmitz, G. M. Ogg, Eds. (Elsevier, 2020), pp. 309–343. doi: 10.1016/B978-0-12-824360-2.00011-5
74. X. Chen, Y. Zhou, G. A. Shields, Progress towards an improved Precambrian seawater $^{87}Sr/^{86}Sr$ curve. *Earth Sci. Rev.* **224**, 103869 (2022). doi: 10.1016/j.earscirev.2021.103869
75. Ú. C. Farrell *et al*., The sedimentary geochemistry and paleoenvironments project. *Geobiology* **19**, 545–556 (2021). doi: 10.1111/gbi.12462; pmid: 34219351
76. N. J. Planavsky, The elements of marine life. *Nat. Geosci.* **7**, 855–856 (2014). doi: 10.1038/ngeo2307
77. D. E. Canfield *et al*., Highly fractionated chromium isotopes in Mesoproterozoic-aged shales and atmospheric oxygen. *Nat. Commun.* **9**, 2871 (2018). doi: 10.1038/s41467-018-05263-9; pmid: 30030422
78. C. C. Loron *et al*., Early fungi from the Proterozoic era in Arctic Canada. *Nature* **570**, 232–235 (2019). doi: 10.1038/s41586-019-1217-0; pmid: 31118507
79. T. M. Gibson *et al*., Precise age of *Bangiomorpha pubescens* dates the origin of eukaryotic photosynthesis. *Geology* **46**, 135–138 (2018). doi: 10.1130/G39829.1
80. T. Bosak *et al*., Possible early foraminiferans in post-Sturtian (716–635 Ma) cap carbonates. *Geology* **40**, 67–70 (2012). doi: 10.1130/G32535.1
81. S. M. Porter, R. Meisterfeld, A. H. Knoll, Vase-shaped microfossils from the Neoproterozoic Chuar Group, Grand Canyon: A classification guided by modern testate amoebae. *J. Paleontol.* **77**, 409–429 (2003). doi: 10.1666/0022-3360(2003)077<0409:VMFTNC>2.0.CO;2
82. L. A. Riedman, S. M. Porter, C. R. Calver, Vase-shaped microfossil biostratigraphy with new data from Tasmania, Svalbard, Greenland, Sweden and the Yukon. *Precambrian Res.* **319**, 19–36 (2018). doi: 10.1016/j.precamres.2017.09.019
83. J. Beghin *et al*., Microfossils from the late Mesoproterozoic–early Neoproterozoic Atar/El Mreïti Group, Taoudeni Basin, Mauritania, northwestern Africa. *Precambrian Res.* **291**, 63–82 (2017). doi: 10.1016/j.precamres.2017.01.009
84. F. Zhao, M. Zhu, S. Hu, Community structure and composition of the Cambrian Chengjiang biota. *Sci. China Earth Sci.* **53**, 1784–1799 (2010). doi: 10.1007/s11430-010-4087-8
85. C. C. Loron, R. H. Rainbird, E. C. Turner, J. W. Greenman, E. J. Javaux, Implications of selective predation on the macroevolution of eukaryotes: Evidence from Arctic Canada. *Emerg. Top. Life Sci.* **2**, 247–255 (2018). doi: 10.1042/ETLS20170153; pmid: 32412621
86. Q. Tang *et al*., One-billion-year-old epibionts highlight symbiotic ecological interactions in early eukaryote evolution. *Gondwana Res.* **97**, 22–33 (2021). doi: 10.1016/j.gr.2021.05.008
87. P. A. Cohen, J. V. Strauss, A. D. Rooney, M. Sharma, N. Tosca, Controlled hydroxyapatite biomineralization in an ~810 million-year-old unicellular eukaryote. *Sci. Adv.* **3**, e1700095 (2017). doi: 10.1126/sciadv.1700095; pmid: 28782008
88. Q. Tang *et al*., The Proterozoic macrofossil *Tawuia* as a coenocytic eukaryote and a possible macroalga. *Palaeogeogr. Palaeoclimatol. Palaeoecol.* **576**, 110485 (2021). doi: 10.1016/j.palaeo.2021.110485

ACKNOWLEDGMENTS

We thank L. Xue and J. Wang for their assistance with data curation and visualization and Q. Chen and X. Li of the ONEs team at Nanjing University for their assistance with data compiling.
Funding: This research was supported by National Key Research and Development Program of China (2022YFF0800303, 2022YFF0802700, and 2021YFA0718100); National Natural Science Foundation of China (42272001 and 42272005); Fundamental Research Funds for the Central Universities

(0206-14380137 and 0206-14380198 to S.S., F.Z., and Q.T.); Youth Innovation Promotion Association of the Chinese Academy of Sciences (2021307); National Science Foundation (EAR-2021207 to S.X.); Hong Kong RGC-GRF (17316022 to N.R.M. and Q.T.); Jiangsu International Science and Technology Cooperation program (BZ2023068 to S.S.); AI for Science Project of Nanjing University (14380230 to J.F.); the Presidential Postdoctoral Fellowship from the University of Hong Kong to Q.T.; and a postdoctoral fellowship from Research Grants Council of the Hong Kong Special Administrative Region, China (HKU PDFS2122-7S02 to Q.T.). This paper contributes to the Deep-time Digital Earth and OneStratigraphy projects. **Author contributions:** Conceptualization: Q.T. and S.X. Data curation: Q.T., W.Z., L.A.R., and K.P. Methodology: Q.T., W.Z., S.Z., X.H., S.S., S.X., and J.F. Project administration: Q.T. Investigation: Q.T. Visualization: Q.T. and S.Z. Writing – original draft: Q.T. Writing – review & editing: All authors. **Competing interests:** The authors declare that they have no competing interests. **Data and materials availability:** All data and codes are available in the manuscript, supplementary materials (*29*), and Dryad (*23*).

SUPPLEMENTARY MATERIALS

science.org/doi/10.1126/science.adm9137
Materials and Methods
Supplementary Text
Figs. S1 to S10
Table S1
References (*89*–*114*)
MDAR Reproducibility Checklist

Submitted 13 November 2023; resubmitted 20 April 2024
Accepted 24 October 2024
10.1126/science.adm9137